

# SegMate: Asymmetric Attention-Based Lightweight Architecture for Efficient Multi-Organ Segmentation

Andrei-Alexandru Bunea<sup>1</sup>, Dan-Matei Popovici<sup>1</sup>, Radu Tudor Ionescu<sup>2</sup>

<sup>1</sup>POLITEHNICA Bucharest, <sup>2</sup>University of Bucharest

**Abstract.** State-of-the-art models for medical image segmentation achieve excellent accuracy but require substantial computational resources, limiting deployment in resource-constrained clinical settings. We present SegMate, an efficient 2.5D framework that achieves state-of-the-art accuracy, while considerably reducing computational requirements. Our efficient design is the result of meticulously integrating asymmetric architectures, attention mechanisms, multi-scale feature fusion, slice-based positional conditioning, and multi-task optimization. We demonstrate the efficiency-accuracy trade-off of our framework across three modern backbones (EfficientNetV2-M, MambaOut-Tiny, FastViT-T12). We perform experiments on three datasets: TotalSegmentator, SegTHOR and AMOS22. Compared with the vanilla models, SegMate reduces computation (GFLOPs) by up to  $2.5\times$  and memory footprint (VRAM) by up to  $2.1\times$ , while generally registering performance gains of around 1%. On TotalSegmentator, we achieve a Dice score of 93.51% with only 295MB peak GPU memory. Zero-shot cross-dataset evaluations on SegTHOR and AMOS22 demonstrate strong generalization, with Dice scores of up to 86.85% and 89.35%, respectively. We release our open-source code at <https://github.com/andreibunea99/SegMate>.

**Keywords:** Medical image segmentation · Organ-at-risk delineation · Efficient deep learning · Efficient neural design

## 1 Introduction

Radiation therapy represents a fundamental method in treating cancer, used in approximately 50% of all treatment plans for cancer patients [4]. Precision is critical in the delineation process of target volumes and organs-at-risk (OARs), as an accurate segmentation enables an optimal dose distributed to the targeted tumors, while minimizing the exposure to healthy tissues [1]. Manual segmentation is the golden standard in clinical practice, but the task requires maximal attention, lasting 30-60 minutes per patient [30]. Automated multi-organ segmentation can reduce delineation time from 30-60 minutes to just seconds, cutting resource costs by up to 95%, while also capturing subtle features that are

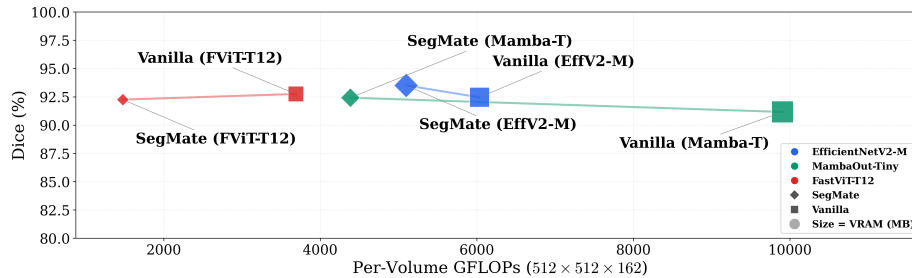


**Fig. 1.** Segmentation accuracy vs. GFLOPs per volume ( $\approx 162$  slices) on TotalSegmentator. Point size indicates VRAM usage. All SegMate variants are below 300 MB.

difficult to identify under clinical time pressure. While state-of-the-art segmentation models achieve high accuracy, they usually require increased computational resources (8–16GB GPU memory), being impractical to be deployed in clinical practice [23]. This creates a deployment and usability barrier that prevents patients from benefiting from cutting-edge AI-assisted solutions.

To bridge the accessibility gap, we propose SegMate, a novel framework that preserves segmentation performance, while significantly reducing compute time and memory footprint (see Fig. 1). Our efficiency-oriented design is based on a meticulous integration of multiple components into a joint framework: (1) early slice fusion via channel attention, (2) asymmetric auto-encoder architecture with a lighter decoder, (3) dual attention mechanisms, (4) multi-scale feature fusion, (4) slice-based positional embeddings, and (5) multi-task optimization.

We carry out experiments on three datasets (TotalSegmentator [34], SegTHOR [20] and AMOS22 [18]) to demonstrate that SegMate can be integrated into various architectures (EfficientNetV2-M [32], MambaOut-Tiny [37], FastViT-T12 [33]) to improve efficiency (in terms of speed and memory), while preserving accuracy. We also show that SegMate leads to improved generalization capacity in zero-shot evaluation setups. Moreover, we perform ablation studies to justify the integration of the proposed components into the joint framework, considering both efficiency and effectiveness.

In summary, our contribution is twofold:

- We introduce SegMate, a novel framework that can be integrated into multiple medical image segmentation models to boost efficiency, while preserving effectiveness.
- To demonstrate the wide applicability of SegMate, we perform comprehensive experiments across multiple datasets, evaluation scenarios, and neural architectures.

## 2 Related Work

Machine learning solutions for segmentation in medical images have significantly improved over the past decades with advances in deep learning architectures and

transformers [22]. The introduction of U-Net [29] marked a cornerstone in precise delineation, leveraging the auto-encoder architecture to capture features at various scales in images. U-Net is a widely used baseline in state-of-the-art solutions, with many best-performing ML models using an enhanced variant from the original structure (e.g. U-Net++ [39] with nested skip pathways, Attention U-Net [25] with attention gates, and 3D U-Net [3]). nnU-Net [17] demonstrates that extensive data preprocessing could drive the performance even higher, enabling an automated hyperparameter optimization mechanism on the training dataset. However, this approach requires substantial computational resources and complex setup procedures. In the last few years, transformer-based architectures like Swin-UNETR [8], TransUNet [2], and UNETR [9] pushed accuracy boundaries (94-95% Dice) at the cost of high GPU memory requirements.

**Foundation models and volumetric adaptation.** VISTA3D [12] establishes a unified 3D segmentation foundation model trained on large-scale annotated CT data. Bio2Vol [40] adapts BiomedParse, a 2D foundation model, to volumetric segmentation, achieving 85.45% Dice across 15 AMOS22 organs, though at substantially higher computational cost than task-specific models. The Post-Axial Refiner (PaR) [15] takes a different angle: it disentangles axial-plane features through a plug-and-play module appended after decoding. Notably, SegMate achieves per-organ results competitive with these methods, without foundation-model-scale pretraining or 3D convolutions, at a fraction of the GPU memory.

**Efficient architectures in medical imaging.** While scaling deep neural networks by adding hidden layers and increasing parameter counts is the main research focus nowadays, some studies concentrate on creating efficient architectures that can demonstrate equivalent performance to heavy models, but with limited computing and memory resources. Generic architectures, such as EfficientNet [31] and MobileNet [13], have been employed in medical image analysis in previous work [19]. Some recent studies target the efficiency bottleneck from the decoder side. EffiDec3D [27] introduces Base Channel Scaling and High-Resolution Removal to cut decoder parameters by up to 96%, applied as a model-agnostic plugin to SwinUNETR and 3D UX-Net. Its successor, EfficientMedNeXt [28], pairs these decoder optimizations with Dilated Multi-Receptive Field Blocks that capture multi-scale context through parallel dilated convolutions. Both works optimize *decoder channels*. In contrast, SegMate takes a complementary route by optimizing *attention placement* and encoder-decoder asymmetry, keeping the full decoder resolution intact, while reducing activation memory through lightweight Squeeze-and-Excitation (SE) [14] gating.

### 3 Method

**Architecture overview.** SegMate is a collection of architectural changes, a.k.a. bag of tricks [11], aiming to boost the computational speed and reduce the memory footprint of auto-encoders applied in medical image segmentation. Our changes are meticulously designed to make every processing component more efficient, starting from the input and going all the way to the output. For the in-

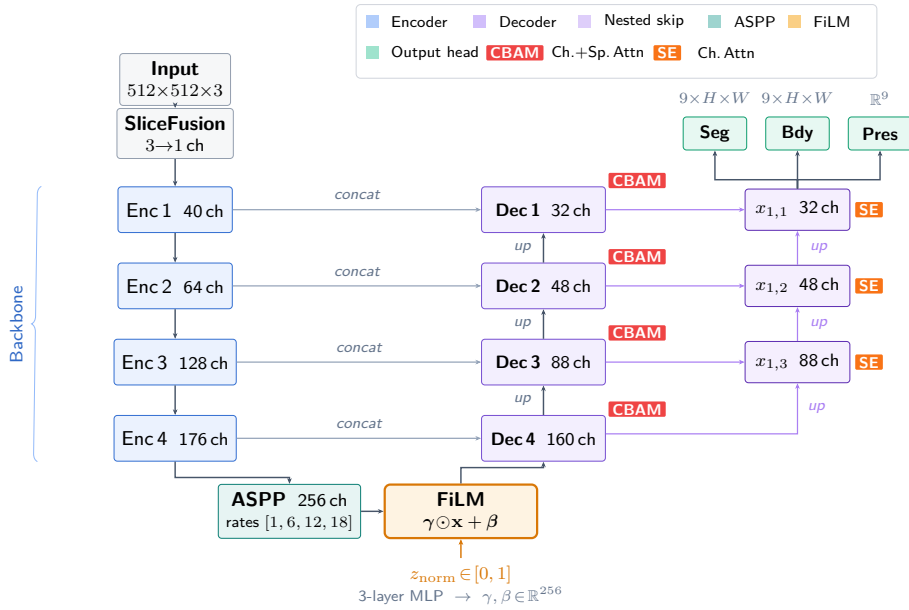


**Fig. 2.** SegMate architecture. CBAM modules are positioned inside the main decoder blocks after encoder-decoder fusion; SE gates nested skip blocks that cascade cross-scale features. FiLM conditions the bottleneck on normalized slice position  $z_{\text{norm}}$ .

put, we introduce SliceFusion, an attention mechanism that fuses the three input slices into a single slice, going from 2.5D to 2D processing. For the architecture, we introduce several changes: (1) an asymmetric encoder-decoder design with a lighter decoder, (2) Squeeze-and-Excitation (SE) [14] blocks in dense decoder skip connections for inter-level feature fusion, (3) Convolutional Block Attention Module (CBAM) [35] in the main decoder path for encoder-decoder integration, (4) slice-positional encoding via Feature-wise Linear Modulation (FiLM) [26]. For the output, we attach three prediction heads that produce segmentation masks, organ boundaries, and organ presence maps. The overall architecture is illustrated in Fig. 2.

**2.5D to 2D.** While 3D networks provide full volumetric context, they impose prohibitive memory costs. 2.5D approaches process stacks of adjacent slices, offering a middle ground between pure 2D efficiency and 3D spatial awareness [7]. We confer vertical (axial) spatial information to our architecture using a 2.5D approach. However, we apply SliceFusion, an attention mechanism that fuses the three input slices into a single slice, thus going from 2.5D to 2D processing for the entire architecture. For each target slice  $t$ , we stack three adjacent axial slices ( $t-1, t, t+1$ ) as an input tensor. Our learned fusion module (SliceFusion) comprises a 2D conv layer with 16 filters of  $3 \times 3$ , a batch normalization layer, a SiLU activation layer, and another 2D conv layer with one filter of  $1 \times 1$ . SliceFusion keeps the processing to a minimum, while still harnessing 2.5D information.

**Slice positional conditioning.** Since our architecture does not process entire volumes, segmentation performance can be affected. To leverage spatial coherence across the Z-axis without explicit 3D convolutions, we introduce Feature-wise Linear Modulation (FiLM) [26] conditioning on the normalized slice position  $z_{norm} \in [0, 1]$ , computed as the relative position of each slice within the patient-specific volume extent. After the ASPP bottleneck [5], we apply a learned affine transformations conditioned on slice position:

$$\mathbf{y} = \gamma(z_{norm}) \odot \mathbf{x} + \beta(z_{norm}), \quad (1)$$

where  $\mathbf{x} \in \mathbb{R}^{H \times W \times C}$  are the bottleneck features,  $\gamma, \beta : [0, 1] \rightarrow \mathbb{R}^C$  are learned functions implemented as three-layer MLPs with hidden dimension 128, and  $\odot$  denotes element-wise multiplication. This modulation allows the network to implicitly learn organ appearance variations across different anatomical levels (e.g. upper vs. lower thorax) without increasing inference memory or requiring 3D convolutions.

**Synergic dual-attention design.** Attention-based segmentation models generally apply a single attention mechanism uniformly throughout the network [6]. Instead, we propose a dual-attention design, assigning distinct roles to SE and CBAM blocks. Our nested decoder implements dense skip connections between adjacent decoder levels, similar to a pruned UNet++. At each nested node, SE blocks [14] perform channel-wise recalibration: global average pooling compresses spatial information into a channel descriptor, which is mapped by a two-layer bottleneck (with  $16\times$  reduction) to per-channel gates. This lightweight gating selects informative features during iterative cross-scale fusion from adjacent decoder levels without significant computational overhead. In the main decoder path, encoder features are concatenated with up-sampled decoder features and passed through CBAM [35]. Beyond channel recalibration, CBAM adds a spatial attention map that localizes informative regions via average and max pooled projections followed by a  $7\times 7$  convolution. This dual gating with channel and spatial attention recovers fine-grained details lost during downsampling in the encoder path, especially for small organs, e.g. esophagus, trachea, etc.

**Asymmetric architecture.** Inspired by masked auto-encoders [10], we employ an asymmetric design combining a high-capacity encoder paired with a compact decoder (at most 160 channels) via an ASPP bottleneck, allowing SegMate to contain 86% more parameters than the standard U-Net, yet consume less GPU memory. The paradox comes from the SE and CBAM blocks that act as lightweight gating mechanisms, keeping decoder activations small, with a maximum decoder width of 160 channels.

**Multi-task boundary enhancement.** SegMate jointly predicts segmentation masks, organ boundaries, and organ presence using three prediction heads. The total loss is determined using the weighted sum of the losses corresponding to each head:

$$\mathcal{L}_{total} = \lambda_{seg} \mathcal{L}_{seg} + \lambda_{bdy} \mathcal{L}_{bdy} + \lambda_{prs} \mathcal{L}_{prs}. \quad (2)$$

The **segmentation head** combines Dice, focal, and cross-entropy losses:

$$\mathcal{L}_{seg} = \lambda_{Dice} (\alpha \mathcal{L}_{Dice} + (1-\alpha) \mathcal{L}_{focal}) + \lambda_{CE} \mathcal{L}_{CE}, \quad (3)$$

**Table 1.** Dice scores (%) over all organs, across three datasets. For SegTHOR (ST) and AMOS22 (A22), we show zero-shot (ZS) and fine-tuning (FT) transfer from TotalSegmentator. Per-volume GFLOPs for a 512×512×162 CT volume with 162 sequential slices. Best per-backbone is in **bold**. Scores represent averages over 3 runs.

| Backbone    | Method  | TotalSeg     | ST           | ZS           | ST           | FT           | A22           | ZS           | A22 | FT | VRAM | GFLOPs |
|-------------|---------|--------------|--------------|--------------|--------------|--------------|---------------|--------------|-----|----|------|--------|
| EffNetV2-M  | SegMate | <b>93.51</b> | <b>86.85</b> | <b>88.51</b> | <b>89.35</b> | <b>91.29</b> | <b>295 MB</b> | <b>5,097</b> |     |    |      |        |
|             | Vanilla | 92.45        | 85.36        | 88.06        | 89.29        | 91.22        | 374 MB        | 6,034        |     |    |      |        |
| MambaOut-T  | SegMate | <b>92.42</b> | <b>86.46</b> | <b>86.67</b> | <b>89.14</b> | <b>90.44</b> | <b>208 MB</b> | <b>4,384</b> |     |    |      |        |
|             | Vanilla | 91.16        | 83.11        | 86.66        | 88.22        | 90.28        | 431 MB        | 9,905        |     |    |      |        |
| FastViT-T12 | SegMate | 92.25        | <b>84.23</b> | <b>87.13</b> | <b>88.87</b> | <b>91.52</b> | <b>120 MB</b> | <b>1,476</b> |     |    |      |        |
|             | Vanilla | <b>92.75</b> | 83.19        | 86.02        | 88.24        | 88.51        | 253 MB        | 3,688        |     |    |      |        |

where  $\mathcal{L}_{\text{Dice}}$  mitigates class imbalance,  $\mathcal{L}_{\text{focal}}$  emphasizes hard pixels, and  $\mathcal{L}_{\text{CE}}$  stabilizes training. The **boundary head** predicts edge probability maps via a  $1 \times 1$  projection, supervised by Dice loss against Sobel-extracted ground-truth edges. The **presence head** uses global average pooling followed by a fully connected layer to produce a vector  $\hat{p} \in [0, 1]^K$ , trained with binary cross-entropy against  $y_k = \mathbf{1}(\sum Y_{\text{true}}^{(k)} > 0)$ , suppressing false positives on slices where an organ is absent. Here,  $K$  is the number of organs.

## 4 Experiments and Results

**Datasets.** We perform experiments on TotalSegmentator v2.0.1 [34], selecting a subset of 9 organs spanning a wide range of sizes, representative for general assumptions in OAR delineation tasks: left/right lung, spinal cord, esophagus, liver, left/right kidney, aorta and trachea. Patient-level splits gather 804/160/107 patients for train/val/test. We additionally evaluate zero-shot and fine-tuned models on SegTHOR [20] and AMOS22 [18]. SegTHOR is a dataset of 40 CT volumes with annotations for esophagus, aorta and trachea, split at the patient level into train/val/test subsets. AMOS provides 200/100/200 CT scans for train/val/test, each with voxel-level annotations of 15 abdominal organs. We report results on the validation set, as the test set is not publicly available.

**Baseline architectures.** We integrate SegMate into three recent neural architectures: EfficientNetV2-M [32], MambaOut-Tiny [37], FastViT-T12 [33]. We compare the original models (called vanilla) with the SegMate versions.

**Pre-processing, hyperparameter and evaluation settings.** CT scans are processed into slices that are clipped to  $[-1000, 2000]$  HU, normalized to  $[0, 1]$  and resized to  $512 \times 512$ . All models (including baselines) are optimized via AdamW ( $2 \cdot 10^{-4}$  learning rate,  $10^{-4}$  weight decay) with “reduce on plateau” scheduling and per-class loss weights to emphasize small organs and compensate for class imbalance. Training runs for 100 epochs on  $3 \times \text{A100}$  GPUs with DDP and batch size 32. We reconstruct 3D volumes from predicted 2D slices for clinical relevance, and we report 3D volume-level Dice scores. Fine-tuning is performed for 25 epochs, with frozen encoders for the first 5 epochs, and a learning rate

**Table 2.** Comparison with state-of-the-art methods across three datasets (3D volume-level Dice %). ZS: zero-shot transfer from TotalSegmentator; FT: fine-tuned. <sup>†</sup>Models evaluated by PaR [15]. <sup>‡</sup>Models evaluated by Bio2Vol [40]. Best per dataset is in **bold**.

| Method                  | Type | ZS Dice      | FT Dice                  | Train Set                    |
|-------------------------|------|--------------|--------------------------|------------------------------|
| <i>TotalSegmentator</i> |      |              |                          |                              |
| SegMate (EffNetV2-M)    | 2.5D | –            | 93.51                    | TotalSeg                     |
| nnU-Net [17]            | 2D   | –            | <b>94.99</b>             | TotalSeg                     |
| Standard U-Net          | 2D   | –            | 87.48                    | TotalSeg                     |
| <i>SegTHOR</i>          |      |              |                          |                              |
| SegMate (EffNetV2-M)    | 2.5D | <b>86.85</b> | 88.51                    | TotalSeg (ZS) / SegTHOR (FT) |
| SegMate (MambaOut-T)    | 2.5D | 86.46        | 86.67                    | TotalSeg (ZS) / SegTHOR (FT) |
| SegMate (FastViT-T12)   | 2.5D | 84.23        | 87.13                    | TotalSeg (ZS) / SegTHOR (FT) |
| 3D U-Net + PaR [15]     | 3D   | –            | <b>89.82<sup>†</sup></b> | SegTHOR                      |
| MultiResUNet [16]       | 3D   | –            | 88.53 <sup>†</sup>       | SegTHOR                      |
| 3D UX-Net [21]          | 3D   | –            | 87.34 <sup>†</sup>       | SegTHOR                      |
| Swin UNETR [8]          | 3D   | –            | 87.26 <sup>†</sup>       | SegTHOR                      |
| SegResNet [24]          | 3D   | –            | 86.99 <sup>†</sup>       | SegTHOR                      |
| nnFormer [38]           | 3D   | –            | 86.65 <sup>†</sup>       | SegTHOR                      |
| UNETR [9]               | 3D   | –            | 84.03 <sup>†</sup>       | SegTHOR                      |
| <i>AMOS22</i>           |      |              |                          |                              |
| SegMate (EffNetV2-M)    | 2.5D | <b>89.35</b> | 91.29                    | TotalSeg (ZS) / AMOS22 (FT)  |
| SegMate (MambaOut-T)    | 2.5D | 89.14        | 90.44                    | TotalSeg (ZS) / AMOS22 (FT)  |
| SegMate (FastViT-T12)   | 2.5D | 88.87        | <b>91.52</b>             | TotalSeg (ZS) / AMOS22 (FT)  |
| Bio2Vol [40]            | 3D   | –            | 87.84 <sup>‡</sup>       | AMOS22                       |
| SwinUNETR [8]           | 3D   | –            | 84.37 <sup>‡</sup>       | AMOS22                       |
| SegMamba [36]           | 3D   | –            | 84.26 <sup>‡</sup>       | AMOS22                       |
| nnFormer [38]           | 3D   | –            | 83.48 <sup>‡</sup>       | AMOS22                       |
| nnUNet [17]             | 3D   | –            | 76.44 <sup>‡</sup>       | AMOS22                       |

of  $5 \cdot 10^{-6}$ . All evaluations are performed on 1×GeForce RTX 5070 Ti GPU, measuring peak and average efficiency metrics on inference (GFLOPs, VRAM).

**Vanilla vs. SegMate.** In Table 1, we report average Dice over all organs on TotalSegmentator (see third column). SegMate variants outperform vanilla variants for EffNetV2-M and MambaOut-T, with gains ranging from +1.06 (EffNetV2-M) to +1.26 (MambaOut-T), suggesting that our lightweight backbones benefit from the proposed architectural enhancements. Our SegMate (EffNetV2-M) variant reaches the highest Dice score (93.51%) on TotalSegmentator.

**Cross-dataset generalization.** In Table 1, we also report zero-shot and fine-tuning results of the models that have been trained on TotalSegmentator. SegMate (EffNetV2-M) reaches 86.85% zero-shot Dice, a +1.45-point gain over the vanilla EffNetV2-M (85.36%). After fine-tuning, SegMate (EffNetV2-M) achieves a Dice of 88.51%. On AMOS22, SegMate (EffNetV2-M) leads the zero-shot accuracy with 89.35% average Dice across all five organs. After fine-tuning, SegMate (FastViT-T12) achieves the best average Dice (91.52%), demonstrating that the proposed framework can be competitive even with 120 MB memory usage. In general, SegMate reduces GFLOPs by up to 2.5× and VRAM by up to 2.1×, while generally surpassing the vanilla models in terms of Dice.

**Comparison with state of the art.** In Table 2, we compare SegMate against state-of-the-art methods. On TotalSegmentator, SegMate (EffNetV2-M) reaches

**Table 3.** SegMeta ablation for EfficientNetV2-M applied on TotalSegmentator. All results are reported at 2D slice level (organ-averaged). Values after vanilla baseline show absolute percentage point change w.r.t the baseline. Highest gain is in **bold**.

| Measure                   | Vanilla | +Asym. dec.  | +CBAM        | +SE   | +2.5D | +Slice Pos.  |
|---------------------------|---------|--------------|--------------|-------|-------|--------------|
| Dice (%) $\uparrow$       | 92.45   | +0.45        | +0.65        | +0.81 | +0.95 | <b>+1.06</b> |
| HD95 (mm) $\downarrow$    | 4.97    | -0.62        | -0.61        | -0.80 | -0.81 | <b>-0.84</b> |
| VRAM (MB) $\downarrow$    | 373.9   | <b>-85.5</b> | <b>-85.5</b> | -85.4 | -85.4 | <b>-85.5</b> |
| GFLOPs/slice $\downarrow$ | 37.25   | <b>-5.79</b> | -5.78        | -5.78 | -5.78 | -5.78        |

93.51% Dice at 295MB peak VRAM, which is 40-50 $\times$  below the resources needed to run a 12-16GB state-of-the-art model such as Swin UNETR or 3D nnU-Net. On SegTHOR, our fine-tuned SegMate (EffNetV2-M) model (88.51%) surpasses Swin UNETR and nnFormer, falling 1.31% short of 3D U-Net+PaR [15]. On AMOS22, all three zero-shot SegMate variants exceed all state-of-the-art models, indicating that SegMate leads to strong generalization capacity. Fine-tuning on AMOS22 puts an even greater gap in favor of our models.

**Ablation study.** In Table 3, we present an ablation study where we progressively add each SegMate component to the vanilla baseline (EfficientNetV2-M). Our results show that each step improves Dice and HD95, while the asymmetric decoder alone cuts VRAM and GFLOPs by a large extent.

**Efficiency analysis.** In Figure 1, we showcase the efficiency-accuracy trade-off measured on the TotalSegmentator dataset. All three SegMate variants register VRAM below 300MB and Dice scores between 92.2% and 93.6%. SegMate variants based on the FastViT-T12 encoder reach the extreme efficiency end (120 MB VRAM with 1,476 GFLOPs), while maintaining a competitive Dice of 92.25%. To quantify total compute per patient, we measure per-slice GFLOPs and multiply by the average number of axial slices (162 slices on average in our test set). SegMate (FastViT) segments a full volume in 1,476 GFLOPs, while the EffNetV2-M variant requires 5,097 GFLOPs. For comparison, recent efficient 3D methods such as EfficientMedNeXt-Tiny [28] and EffiDec3D [27] report low per-patch costs (7-51 GFLOPs), but sliding-window inference over the same volume size still totals  $\sim$ 1,500-10,000 GFLOPs.

## 5 Conclusion

In this paper, we introduced SegMate, a framework that integrates multiple architectural design changes that target efficiency boosting and effectiveness preservation for organ segmentation in medical images. We presented empirical evidence to demonstrate that SegMate achieves the desired goals across distinct neural architectures, datasets and evaluation setups. Furthermore, we showed the effect of introducing the proposed components via an ablation study, confirming that each component plays a key role in either reducing computation or boosting performance. In future work, we aim to integrate SegMate into additional models and construct a more comprehensive repository of pretrained readily available models at <https://github.com/andreibunea99/SegMate>.

## References

1. Brouwer, C.L., Steenbakkens, R.J., Bourhis, J., et al.: CT-based delineation of organs at risk in the head and neck region: DAHANCA, EORTC, GORTEC, HKN-PCSG, NCIC CTG, NCRI, NRG Oncology and TROG consensus guidelines. *Radiotherapy and Oncology* **117**(1), 83–90 (2015)
2. Chen, J., Lu, Y., Yu, Q., et al.: TransUNet: Transformers make strong encoders for medical image segmentation. arXiv preprint arXiv:2102.04306 (2021)
3. Çiçek, Ö., Abdulkadir, A., Lienkamp, S.S., et al.: 3D U-Net: Learning dense volumetric segmentation from sparse annotation. In: *Proceedings of MICCAI*. pp. 424–432 (2016)
4. Delaney, G., Jacob, S., Featherstone, C., et al.: The role of radiotherapy in cancer treatment: estimating optimal utilization from a review of evidence-based clinical guidelines. *Cancer* **104**(6), 1129–1137 (2005)
5. Ding, P., Qian, H., Zhou, Y., et al.: Real-time efficient semantic segmentation network based on improved ASPP and parallel fusion module in complex scenes. *Journal of Real-Time Image Processing* **20**(3), 41 (2023)
6. Georgescu, M.I., Ionescu, R.T., Miron, A.I., et al.: Multimodal multi-head convolutional attention with various kernel sizes for medical image super-resolution. In: *Proceedings of WACV*. pp. 2195–2205 (2023)
7. Han, Z., Wei, B., Leung, S., et al.: Spine-GAN: Semantic segmentation of multiple spinal structures. *Medical Image Analysis* **50**, 23–35 (2021)
8. Hatamizadeh, A., Nath, V., Tang, Y., et al.: Swin UNETR: Swin transformers for semantic segmentation of brain tumors in MRI images. In: *Proceedings of BrainLes*. pp. 272–284 (2022)
9. Hatamizadeh, A., Tang, Y., Nath, V., et al.: UNETR: Transformers for 3D medical image segmentation. In: *Proceedings of WACV*. pp. 574–584 (2022)
10. He, K., Chen, X., Xie, S., et al.: Masked autoencoders are scalable vision learners. In: *Proceedings of CVPR*. pp. 16000–16009 (2022)
11. He, T., Zhang, Z., Zhang, H., et al.: Bag of tricks for image classification with convolutional neural networks. In: *Proceedings of CVPR*. pp. 558–567 (2019)
12. He, Y., Yang, D., Nath, V., et al.: VISTA3D: Versatile imaging segmentation and annotation model for 3D computed tomography. In: *Proceedings of CVPR* (2025)
13. Howard, A.G., Zhu, M., Chen, B., et al.: MobileNets: Efficient convolutional neural networks for mobile vision applications. In: arXiv preprint arXiv:1704.04861 (2017)
14. Hu, J., Shen, L., Sun, G.: Squeeze-and-excitation networks. In: *Proceedings of CVPR*. pp. 7132–7141 (2018)
15. Huang, X., Huang, J., Guo, Y., et al.: Volumetric axial disentanglement enabling advancing in medical image segmentation. In: *Proceedings of IJCAI*. pp. 1197–1205 (2025)
16. Ibtihaz, N., Rahman, M.S.: MultiResUNet: Rethinking the U-Net architecture for multimodal biomedical image segmentation. *Neural Networks* **121**, 74–87 (2020)
17. Isensee, F., Jaeger, P.F., Kohl, S.A., et al.: nnU-Net: a self-configuring method for deep learning-based biomedical image segmentation. *Nature Methods* **18**(2), 203–211 (2021)
18. Ji, Y., Bai, H., Yang, J., et al.: AMOS: A large-scale abdominal multi-organ benchmark for versatile medical image segmentation. In: *Proceedings of NeurIPS*. pp. 36722–36732 (2022)
19. Kuş, Z., Aydın, M.: MedSegBench: A comprehensive benchmark for medical image segmentation in diverse data modalities. *Scientific Data* **11**(1), 1283 (2024)

20. Lambert, Z., Petitjean, C., Dubray, B., et al.: SegTHOR: Segmentation of thoracic organs at risk in CT images. *Medical Image Analysis* (2020)
21. Lee, H.H., Bao, S., Gong, Y., et al.: 3D UX-Net: A large kernel volumetric ConvNet modernizing hierarchical transformer for medical image segmentation. In: *Proceedings of ICLR* (2023)
22. Litjens, G., Kooi, T., Bejnordi, B.E., et al.: A survey on deep learning in medical image analysis. *Medical Image Analysis* **42**, 60–88 (2017)
23. Ma, J., Zhang, Y., Gu, S., et al.: Fast and low-GPU-memory abdomen CT organ segmentation: The FLARE challenge. *Medical Image Analysis* **82**, 102616 (2022)
24. Myronenko, A.: 3D MRI brain tumor segmentation using autoencoder regularization. In: *Proceedings of BrainLes*. pp. 311–320 (2019)
25. Oktay, O., Schlemper, J., Folgoc, L.L., et al.: Attention U-Net: Learning where to look for the pancreas. In: *Proceedings of MIDL* (2018)
26. Perez, E., Strub, F., De Vries, H., et al.: FiLM: Visual reasoning with a general conditioning layer. In: *Proceedings of AAAI*. vol. 32 (2018)
27. Rahman, M.M., Marculescu, R.: EffiDec3D: An optimized decoder for high-performance and efficient 3D medical image segmentation. In: *Proceedings of CVPR*. pp. 10435–10444 (2025)
28. Rahman, M.M., Munir, M., Marculescu, R.: EfficientMedNeXt: Multi-receptive dilated convolutions for medical image segmentation. In: *Proceedings of MICCAI*. pp. 193–203 (2025)
29. Ronneberger, O., Fischer, P., Brox, T.: U-Net: Convolutional networks for biomedical image segmentation. In: *Proceedings of MICCAI*. pp. 234–241 (2015)
30. Sharp, G., Fritscher, K.D., Pekar, V., et al.: Vision 20/20: perspectives on automated image segmentation for radiotherapy. *Medical Physics* **41**(5), 050902 (2014)
31. Tan, M., Le, Q.: EfficientNet: Rethinking model scaling for convolutional neural networks. In: *Proceedings of ICML*. pp. 6105–6114 (2019)
32. Tan, M., Le, Q.V.: EfficientNetV2: Smaller models and faster training. In: *Proceedings of ICML*. pp. 10096–10106 (2021)
33. Vasu, P.K.A., Gabriel, J., Zhu, J., et al.: FastViT: A fast hybrid vision transformer using structural reparameterization. In: *Proceedings of ICCV*. pp. 5785–5795 (2023)
34. Wasserthal, J., Breit, H.C., Meyer, M.T., et al.: TotalSegmentator: robust segmentation of 104 anatomic structures in CT images. *Radiology: Artificial Intelligence* **5**(5), e230024 (2023)
35. Woo, S., Park, J., Lee, J.Y., Kweon, I.S.: CBAM: Convolutional block attention module. In: *Proceedings of ECCV*. pp. 3–19 (2018)
36. Xing, Z., Ye, T., Yang, Y., et al.: SegMamba: Long-range sequential modeling Mamba for 3D medical image segmentation. In: *Proceedings of MICCAI*. pp. 578–588 (2024)
37. Yu, W., Wang, X.: MambaOut: Do we really need Mamba for vision? *arXiv preprint arXiv:2405.07992* (2024)
38. Zhou, H.Y., Guo, J., Zhang, Y., et al.: nnFormer: Volumetric medical image segmentation via a 3D transformer. *IEEE Transactions on Image Processing* **32**, 4036–4045 (2023)
39. Zhou, Z., Siddiquee, M.M.R., Tajbakhsh, N., et al.: UNet++: A nested U-Net architecture for medical image segmentation. *Proceedings of DLMIA* pp. 3–11 (2018)
40. Zhuang, Y., He, Y., Yang, D., et al.: From biomedical image to volumetric medical image: A universal 3D segmentation method. In: *Proceedings of MICCAI* (2025)